

Experimental Study of the $K_{\mu 3}^0$ Form Factors

P. BASILE, J. W. CRONIN,* B. THEVENET, R. TURLAY, S. ZYLBERAJCH, AND A. ZYLBERSZTEJN

Department de Physique des Particules Élémentaires, CEN Saclay, France

(Received 21 April 1969; revised manuscript received 17 March 1970)

A spark-chamber experiment is described which measured the distribution in the Dalitz plot of 3140 $K_{\mu 3}^0$ decays, and measured the branching ratio $\Gamma(K_L \rightarrow \pi\mu\nu)/\Gamma(K_L \rightarrow \pi e\nu)$. From a study of the Dalitz plot, a ratio of form factors $\xi = -3.9 \pm 0.4$ is found with little or no energy dependence. The branching-ratio measurement gives a value $\xi = -0.5 \pm 0.5$ which is incompatible with the Dalitz-plot result. The results are discussed from the point of view of possible experimental bias. The results are compared with other experiments.

I. INTRODUCTION

THE decay mode $K \rightarrow \pi\mu\nu$ for both charged and neutral mesons has been studied continuously since the discovery of K mesons.^{1,2} Recently there has been significant experimental controversy concerning this decay mode as the precision of various experiments has improved. We briefly review the main phenomenological features of this decay mode in the paragraphs which follow.

If a vector interaction is assumed, then the decay amplitude for $K_L \rightarrow \pi l\nu$ can be written³

$$M = \sum_{\alpha} f_{+}(q^2)(P_K + P_{\pi})_{\alpha} + f_{-}(q^2)(P_K - P_{\pi})_{\alpha} \\ \times \bar{u}_l \gamma_{\alpha} (1 + \gamma_5) u_{\nu}.$$

Here $f_{+}(q^2)$ and $f_{-}(q^2)$ are the two possible vector form factors which are scalar functions of the four-momentum transfer in the decay. P_K and P_{π} are the four-momenta of the K meson and pion, respectively. The four-momentum transfer is given by

$$q^2 = -(P_K - P_{\pi})^2 = M_K^2 + M_{\pi}^2 - 2M_K E_{\pi}^*,$$

where E_{π}^* is the total pion energy in the K -meson rest system. When the matrix element is evaluated, the $f_{-}(q^2)$ term is multiplied by m_l/m_K , which makes its contribution negligible when the lepton is an electron.

If universality between electron and muon is assumed, then $f_{+}(q^2)$ is determined from a study of $K_L \rightarrow \pi e\nu$ (K_{e3}). A compilation of recent experiments,³⁻⁷ including one⁸ carried out with the same apparatus used in the experiment reported here, finds $f_{+}(q^2)$ to have a q^2

dependence given by

$$f_{+}(q^2) = f_{+}(0)[1 + (0.020 \pm 0.008)q^2/m_{\pi}^2],$$

where the form-factor dependence $\lambda_{+} = 0.020 \pm 0.008$ is a weighted average of the above experiments. Study of the $K_L \rightarrow \pi\mu\nu$ ($K_{\mu 3}$) decay mode yields a result which is usually expressed in terms of the ratio of form factors

$$\xi(q^2) = f_{-}(q^2)/f_{+}(q^2).$$

The form factor $\xi(q^2)$ can be determined in three distinct ways:

(1) Measurement of the branching ratio $\Gamma(K_{\mu 3})/\Gamma(K_{e3})$. Under the assumption of electron-muon universality, $\xi(0)$ can be determined directly from the branching ratio, provided that one knows that the form-factor dependence is small. Or, by comparison of the partial rate of $K_{\mu 3}$ at a particular q^2 to the corresponding rate of K_{e3} , $\xi(q^2)$ can be determined.

(2) Measurement of the distribution of $K_{\mu 3}$ events on a Dalitz plot. This method is independent of the universality assumption but requires precise knowledge of the relative detection efficiency of the apparatus over the Dalitz plot.

(3) Measurement of the muon total polarization in the decay. This method is also independent of the universality assumption and only requires a detector of muon polarization.

In this experiment we have undertaken the measurement of $\xi(q^2)$ by the first two methods stated above.

The distribution of events on the Dalitz plot is given by

$$\frac{dW(E_{\pi}^*, E_{\mu}^*)}{dE_{\pi}^* dE_{\mu}^*} = f_{+}(q^2)[A + B \operatorname{Re}(\xi(q^2)) \\ + C|\xi(q^2)|^2], \quad (1)$$

where

$$A = M_{\mu}^2(W - E_{\pi}^* - 4E_{\nu}^*) \\ + 4M_K[M_K(E_{\pi}^* - W) + 2E_{\mu}^*E_{\nu}^*],$$

$$B = 2M_{\mu}^2(E_{\pi}^* - W) + 4M_{\mu}^2E_{\nu}^*,$$

$$C = M_{\mu}^2(W - E_{\pi}^*),$$

$$W = (M_K^2 + M_{\pi}^2 - M_{\mu}^2)/2M_K,$$

$$E_{\nu}^* = M_K - E_{\pi}^* - E_{\mu}^*.$$

* Present address: Jadwin Hall, Princeton, N. J.

¹ A survey of experimental work prior to 1964 is given in the review article by T. D. Lee and C. S. Wu, *Ann. Rev. Nucl. Sci.* **15**, 381 (1965).

² References subsequent to 1965 are given in Table VIII of D. Cutts, R. Stiening, C. Wiegand, and M. Deutsch, *Phys. Rev.* **184**, 1380 (1969).

³ S. W. MacDowell, *Nuovo Cimento* **6**, 1445 (1957).

⁴ A. Firestone, J. K. Kim, J. Lach, J. Sandweiss, H. D. Taft, and P. Guidoni, *Phys. Rev. Letters* **18**, 176 (1967).

⁵ J. P. Lowys, B. Aubert, L. M. Chounet, and C. Pascaud, *Phys. Letters* **24B**, 75 (1967).

⁶ J. A. Kadyk, J. H. Chan, D. Drijard, Y. Oren, and B. M. Sheldon, *Phys. Rev. Letters* **19**, 597 (1967).

⁷ S. H. Aronson and K. W. Chen, *Phys. Rev. Letters* **20**, 287 (1968).

⁸ P. Basile, J. W. Cronin, B. Thevenet, R. Turlay, S. Zylberajch, and A. Zylbersztein, *Phys. Letters* **26B**, 542 (1968).

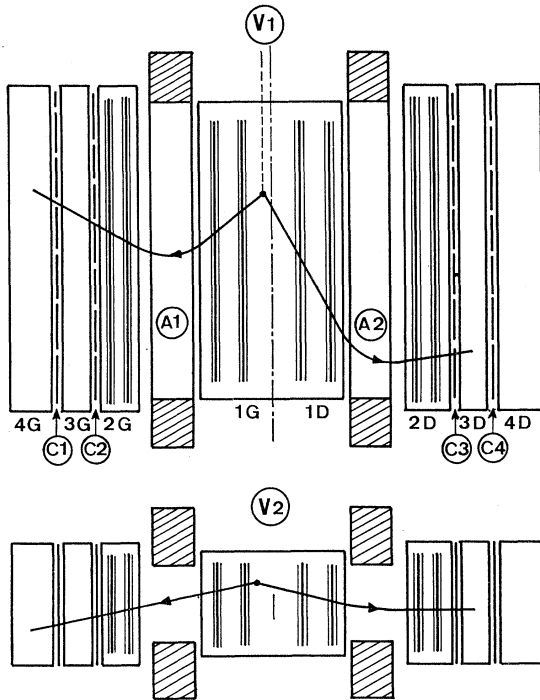


FIG. 1. Schematic view of experimental apparatus. V_1 is a view from above; V_2 is a view looking upstream. The symbols have the following meaning: A_i , momentum-analyzing magnets; C_i , scintillation counters for trigger; 1G, 2G, 1D, and 2D, thin-foil spark chambers for momentum analysis; 3G, 4G, 3D, and 4D, range chambers for particle identification.

With the apparatus described below, we identify and observe events over a large portion of the Dalitz plot. The efficiency, however, is not constant over the plot, and must be evaluated by Monte Carlo techniques. These Monte Carlo calculations are discussed in the Appendix.

II. APPARATUS

A beam of K_L was produced by 3-BeV protons striking a uranium target in Saturne. The K_L of mean momentum 250 MeV/c were defined by a channel at 90° to the incident protons and passed through the detection apparatus at 7 m from the target. A schematic view of the apparatus is shown in Fig. 1. It consisted of two thin-foil spark chambers (1G and 1D) placed on either side of the beam. Two long magnets with an aperture of 150×30 cm and 40-cm thickness were placed just beyond the thin-foil chambers. These magnets were followed by two more thin-foil chambers (2G and 2D). This arrangement allowed the measurement of decay-product momenta with a standard error of 3%.

The identification of the decay products into categories π , μ , or e was accomplished by range chambers which followed the thin-foil chambers. On each side, a 2×1 -m scintillator array C_i was followed by a

20-g/cm² steel chamber (3G or 3D). Another scintillator bank followed by a 90-g/cm² brass chamber (4G or 4D) completed the apparatus. The thickness of the plates was graduated in such a way that there was at least one spark difference in the range between pions and muons of the same momentum. The one-spark margin was maintained as long as the error in the momentum determination was less than about 5%. Figure 2 shows the location of the range-chamber plates in equivalent thickness of copper against the range curves for pions and muons.

The spark chambers were triggered by a coincidence between C_1 and C_2 and by the requirement that one of the two decay products penetrate 20 g/cm² of steel. The data were recorded on film. Measurements of the spectrometer tracks were made with the help of an automatic film-measuring system "Ariane." The range of the decay products was determined by hand measurement and the final identification by physicists.

III. ANALYSIS

A. Calibration of Spectrometer

We have used regeneration of K_S to determine experimentally the precision in measurement of the vector momentum of the decay products. A 5-cm copper regenerator was placed at the entrance of the apparatus. The $K_S \rightarrow \pi^+\pi^-$ decays are expected to

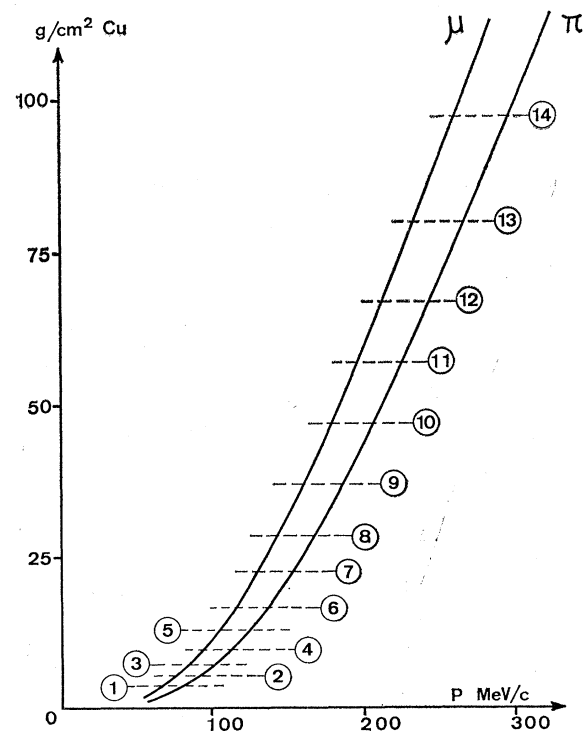


FIG. 2. Range curves for μ 's and π 's in copper. The dotted lines show the equivalent range in copper for each gap of the range chamber for the case of a track incident perpendicular to the chamber.

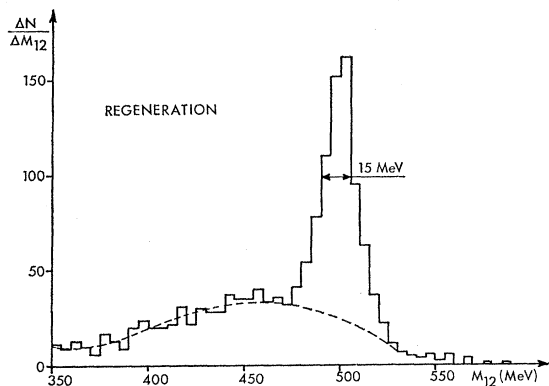


FIG. 3. $M_{\pi\pi}$ distribution for events within 10 cm downstream from a copper regenerator. Dashed curve is expected from K_L decay alone.

show an effective-mass peak at 498 MeV and the sum of the vector momenta of the two decay pions is expected to be aligned with the incident beam. The widths of these distributions can be directly related to the errors in the momenta and directions of the decay particles.

Figure 3 shows a plot of the effective $\pi\pi$ mass distribution for all events with decay vertices within 10 cm of the regenerator. The dashed curve is the distribution found for only K_L decays normalized to events below $M_{\pi\pi} = 450$ MeV. The excess distribution shows a mass peak centered at 500 ± 1.5 MeV with a width characterized by a standard deviation of 8 MeV.

Figure 4 shows a plot of the angular distribution of the vector momenta of the two charged particles indicating the sharp angular distribution of the regenerated events. The dashed curve is the distribution expected from free decay. The width of the distribution corresponds to an angular precision of 0.030 rad or an error in transverse momentum of 7.5 MeV/c.

B. Identification of Particles

We have checked the ability of the range chambers to identify electrons, pions, and muons by the performance of an auxiliary experiment. The range chamber was placed in a beam of either pions, muons, or electrons at momenta of 120, 200, 270, and 350 MeV/c. The beam was defined by means of a Čerenkov counter. A pure beam of electrons was obtained with great ease, but the beam of pions and muons had significant contaminations of muons and pions, respectively. In particular, it was difficult to define a beam of muons without a lower-energy component. Nevertheless, the results of these tests indicate that the particle separation method does in fact work.

Figures 5(a) and 5(b) show the result, for 120-MeV/c and 200-MeV/c electrons. Below 150 MeV/c, the electrons do not develop manifest showers but do give a range which exceeds that of a pion or muon. Above

200 MeV, the electrons show a manifest shower in 92% of the cases. The remaining electron events which are plotted in Fig. 5(b) show ranges that are predominantly longer than a muon or pion of the same momentum. Figures 5(c) and 5(d) show the distribution in range for pions and muons. The range of the highest-momentum muons shows a one-spark separation as is expected. The overlap of the pion and muon range is due to the low-energy tail of the muon beam. The long tail of the pion range distribution is due to nuclear interactions.

During the actual experiment, the gap efficiency of the chambers was monitored with cosmic rays and all portions of the data where the quality of the range chambers was suspect were removed from further consideration. Of the events remaining, there were 8% which were impossible to identify. The laboratory momentum distributions of the unidentified events were identical with the identified events, indicating that the failure in identification was not strongly momentum dependent.

The contamination of incorrectly identified events has been evaluated statistically and is described in Sec. III D.

C. Kinematic Reconstruction and Cuts

The knowledge of the K_L line of flight and the momentum and identification of the two charged particles

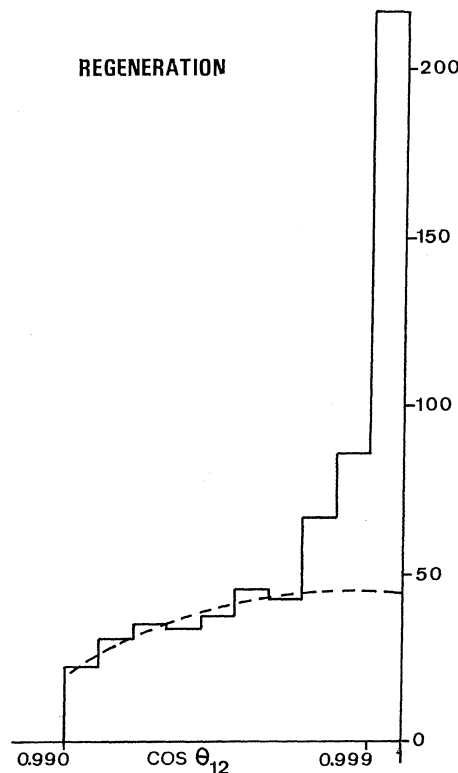


FIG. 4. Angular distribution of the vector sum of the momenta of the two charged particles for events within 10 cm downstream from a copper regenerator.

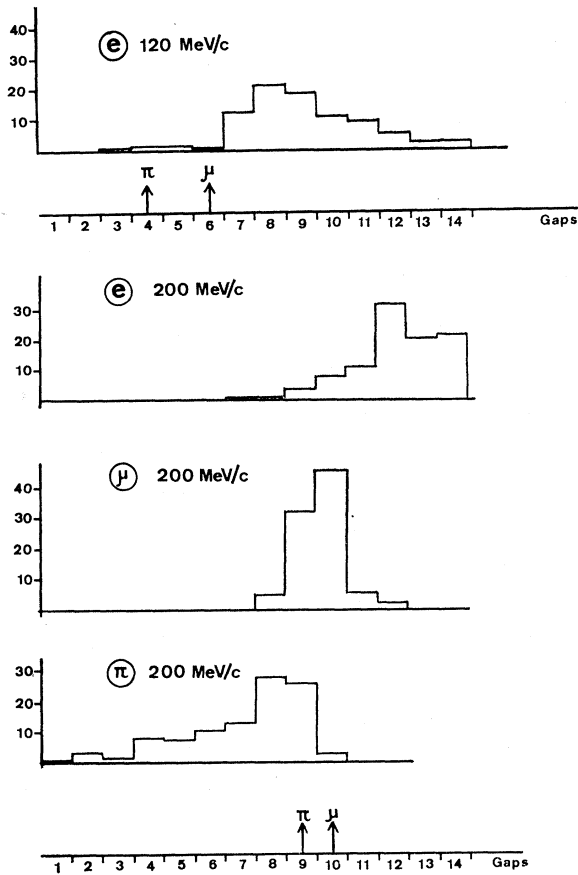


FIG. 5. Results of auxiliary experiment to study particle separation in the range chambers. Details are discussed in the text.

leads to a kinematic fit of zero constraint. In this fit, the sum of the center-of-mass energy of the pion and the muon can be found, as well as the transverse component of the neutrino momentum. The sign of the longitudinal component of the neutrino momentum is unknown, which leads to two choices for the center-of-mass energy of each decay product. The apparatus favors events in which the difference in energy of the two solutions $|E_{\pi}^*(1) - E_{\pi}^*(2)| \leq 20$ MeV in 85% of the cases. Here $E_{\pi}^*(1)$ and $E_{\pi}^*(2)$ are the pion center-of-mass energies for the two solutions, respectively. This distribution is plotted in Fig. 6. As a consequence of the near equality of the two solutions, we take the average of the two values in most of the subsequent analysis.

We have eliminated events for which the quantity $dP = P_0^* - P_T$ was less than -20 MeV/c, where P_0^* is the magnitude of the neutrino momentum in the center-of-mass system which can be calculated from the effective mass of the π - μ system and P_T is the transverse component of the momentum of the two charged particles in the laboratory. With no measurement error, dP must be positive. Those events with dP positive lead to two solutions in the center-of-mass system. The events with $dP=0$ correspond to events

for which the neutrino is exactly transverse and give a single solution. For those events accepted with dP negative, a single solution is found by setting $dP=0$.

The following additional cuts were made:

(1) Events were suppressed which, owing to measurement errors, lay outside the physical limits of the Dalitz plot.

(2) Events were suppressed for which

$$|E_{\pi}^*(1) - E_{\pi}^*(2)| \geq 20 \text{ MeV}.$$

(3) Events were suppressed for those events whose kinematics were consistent with $K_L \rightarrow \pi^+\pi^-\pi^0$ when the particle identification was ignored.

After these cuts were imposed 3140 events remained for analysis: 1575 $K_L \rightarrow \pi^+\mu^-\nu$ and 1565 $K_L \rightarrow \pi^-\mu^+\nu$.

D. Evaluation of Contamination

There are several processes by which events can be included in the $K_{\mu 3}$ sample which are, in fact, other decay modes. Events of the type $K_L \rightarrow \pi^+\pi^-\pi^0$ are particularly serious since they fall in a very limited part of the $K_{\mu 3}$ Dalitz plot when analyzed as $K_{\mu 3}$. The contamination of these events is negligible, because of the cut applied above. A plot of all the data as a function of the quantity⁹ $P_0'^2$ is shown in Fig. 7. There is a clear

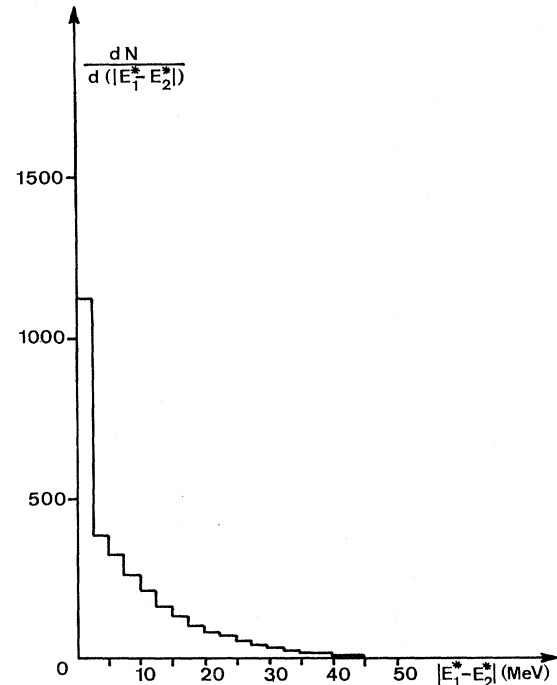


FIG. 6. Experimental distribution of the difference between the two possible energies in the c.m. system for each of the charged secondary particles.

⁹ $P_0'^2$ is the incident K_L momentum in a system where the longitudinal momentum of the two charged particles, when assumed to be pions, is zero. See also Ref. 17.

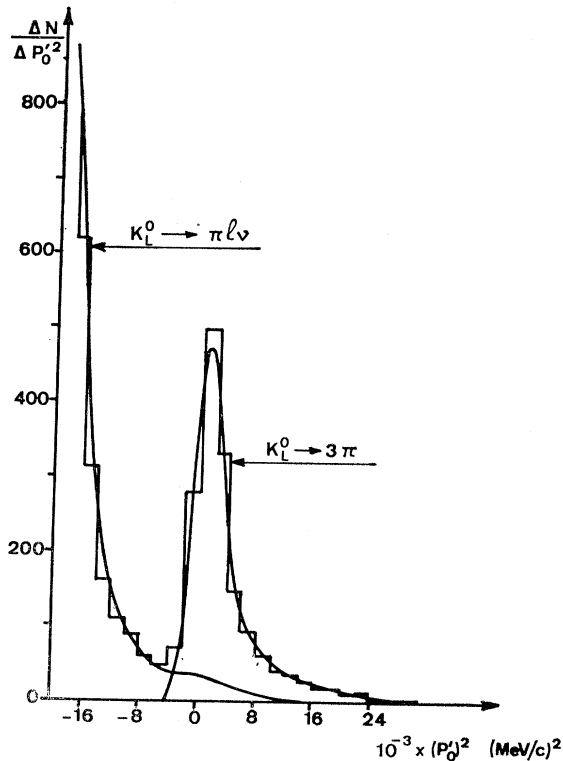


FIG. 7. Histogram of $P_0'^2$ distribution for all events. The solid curves were calculated by the Monte Carlo method.

separation of the $K_L \rightarrow \pi^+\pi^-\pi^0$ events from the K_{L3} events. A similar curve for the identified $K_{\mu 3}$ events is shown in Fig. 8(a) where a cut in $P_0'^2 \geq 0$ has been made. By comparison of the two figures it is clear that the contamination of $K_L \rightarrow \pi^+\pi^-\pi^0$ is negligible.

We have evaluated statistically the contamination of K_{e3} in the $K_{\mu 3}$ sample. To accomplish this, we made use of the fact that the expected distribution of $P_0'^2$ and P_T is different for the two decay modes. Figures 8(a) and 8(b) show the respective distributions expected for $K_{\mu 3}$ (solid line) and K_{e3} (dashed line). The expected distributions are insensitive to variation in the form factors. Using these data, one finds by a least-squares fit that the fraction of K_{e3} in the $K_{\mu 3}$ sample is $(1 \pm 1)\%$.

Because of imperfections in the particle identification, one expects a small fraction of events for which the pion and muon identification is inverted. This inversion requires the misidentification of both particles. We have estimated the probability of a double error in identification giving rise to an inverted event to be about 1%.

We have also examined the 1400 unidentified events to assure that their loss from various parts of the $K_{\mu 3}$ Dalitz plot is reasonably uniform. Figure 9 compares the laboratory spectra for the unidentified events with that of the entire sample. Since the laboratory spectra of these events are identical with the entire sample, we assume that there is no systematic loss of real $K_{\mu 3}$ events from a particular part of the Dalitz plot.

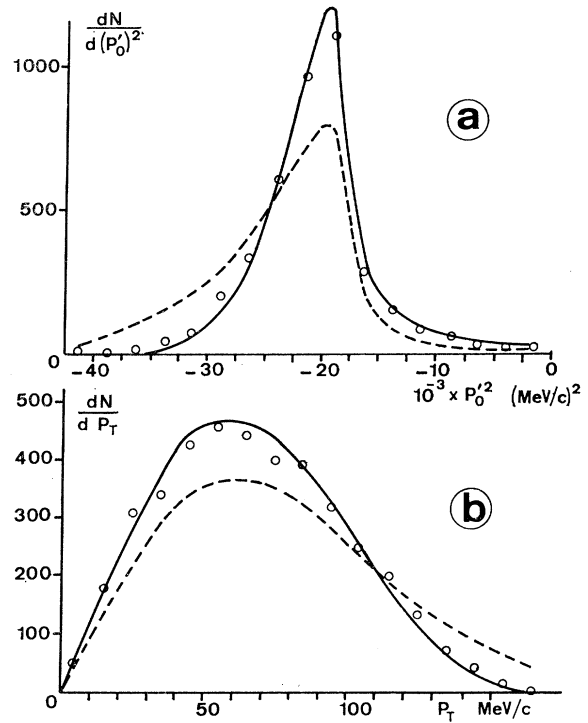


FIG. 8. (a) Distribution of $P_0'^2$ for identified $K_{\mu 3}$ events; (b) distribution of P_T for identified $K_{\mu 3}$ events. The open circles are the experimental values. The solid curves are the expected distributions for $K_{\mu 3}$ and the dashed curves are the expected distributions for K_{e3} .

Finally, we have found by Monte Carlo calculation that an addition of as much as 3% K_{e3} events or 3% inverted events has a negligible effect on the results of the experiment.

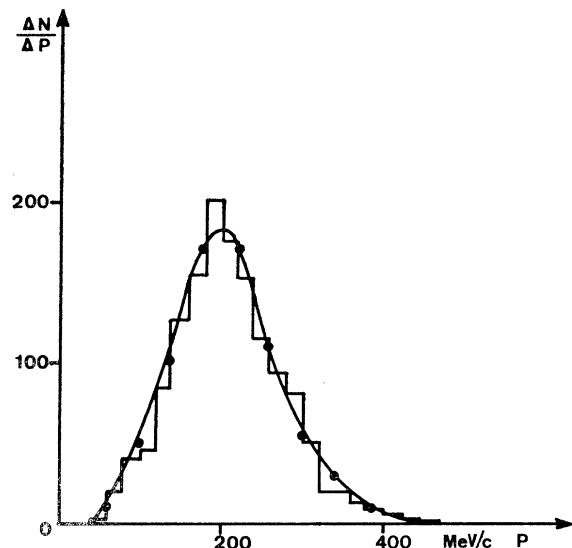


FIG. 9. Momentum distribution in the laboratory for the charged secondaries. The histogram is for the 1418 unidentified events, and the solid curve with dots is for all events.

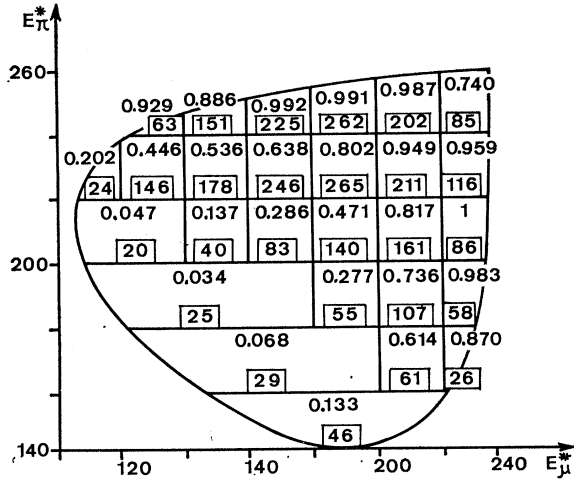


FIG. 10. Relative efficiency of the apparatus as a function of position in the Dalitz plot. The integers in the small boxes are the experimental number of events found in each cell. (Energies in MeV.)

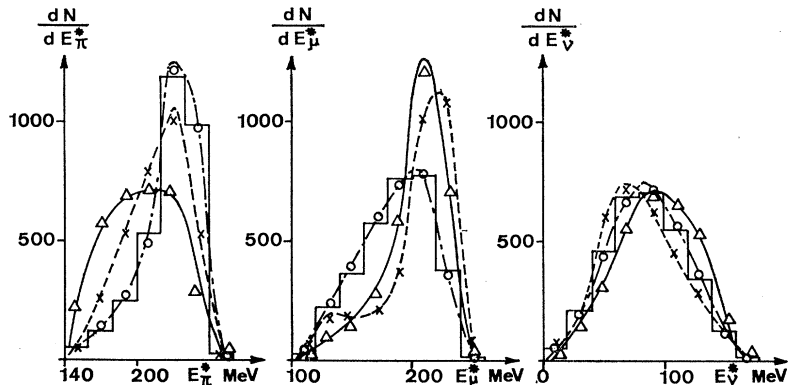
IV. STUDY OF DALITZ PLOT

We have divided the Dalitz plot into cells (i) of dimension 20×20 MeV, where the variables are E_{π}^* and E_{μ}^* , the energy of the pion and muon, respectively, in the center-of-mass system. Cells with a small number of events have been grouped into larger units. We have calculated by the Monte Carlo method the number of events $N_i(x)$ expected in each cell as a function of x , where x symbolizes the set of physical parameters whose values are being sought. Figure 10 shows how we divide the Dalitz plot and gives the number of events found in each cell along with the relative efficiency of the apparatus as a function of position on the Dalitz plot.

In order to test a hypothesis we use the χ^2 technique, in which we minimize the χ^2 by variation of the set of parameters x . We form the quantity

$$\chi^2(x) = \sum_i \frac{[N_i(x) - N_i^{\text{expt}}]^2}{N_i^{\text{expt}}}$$

FIG. 11. Center-of-mass spectra for the three secondary particles. The histograms show the experimental distributions. The expected spectra for the scalar, vector ($\xi = -3.9$), and tensor interaction are shown by the triangles, circles, and crosses, respectively.



¹⁰ See, e.g., S. L. Marateck and S. P. Rosen, Phys. Letters 29B, 497, (1969).

¹¹ K. K. Young, M. J. Longo, and J. A. Helland, Phys. Rev. Letters 18, 806 (1967).

and seek its minimum by variation of the set of parameters x .

A. Nature of Interaction

We have calculated the π , μ , and ν spectra expected on the basis of a pure scalar, vector, or tensor interaction. Of these, only the vector interaction gives a good fit (with $\xi = -3.9$), as can be seen in Fig. 11. Figure 12 shows a plot of the muon spectra for a pion energy range of 230 ± 10 MeV. The fact that no scalar or tensor fit is possible for a narrow range of pion energies makes it very unlikely that such fits could be achieved by suitable q^2 dependence of form factors. For the remainder of this paper we will consider only the vector interaction and will assume that there is no admixture of scalar or tensor. An admixture of scalar interaction is inseparable from the parameter ξ .¹⁰

B. Value of ξ Assuming Constant Form Factors

Polarization studies have shown that the possible value of $\text{Im}\xi$ is less than 0.1.¹¹ Our experiment is very insensitive to the presence of $\text{Im}\xi$ of that size, and thus throughout our analysis we will assume that ξ is real. The results are entirely consistent with $\text{Im}\xi = 0$.

If we assume that ξ is independent of q^2 , we find $\chi^2(\xi)$ has two minima, as shown in Fig. 13. These minima occur at $\xi = -3.90 \pm 0.11$, with $\chi^2 = 24$, and $\xi = 1.52 \pm 0.18$, with $\chi^2 = 108$ for 25 degrees of freedom. The error is derived from the change in the single parameter required to increase χ^2 by one unit. The predicted number of events for each solution along with the experimental number is presented in Fig. 14 for each cell of the Dalitz plot.

In Fig. 15 we present the χ^2 curves for the μ spectrum alone and the π spectrum alone. In each case there are two minima but only the negative value of ξ gives a consistent result.

We have computed the Dalitz-plot distribution using either the upper solution (forward neutrino in the c.m. system) or the lower solution (backward neutrino

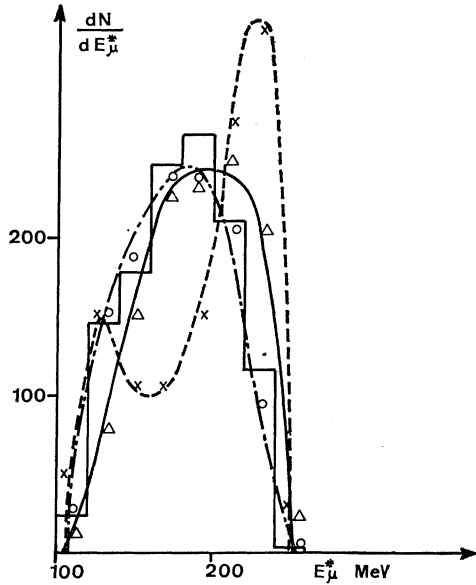


FIG. 12. Muon spectra in the c.m. system for $E_{\pi^*} = 230 \pm 10$ MeV. The expected distribution for the scalar, vector ($\xi = -3.9$), and tensor interaction are shown by the triangles, circles, and crosses, respectively.

in the c.m. system). Then, in the evaluation of the $\chi^2(\xi)$ function, we use the corresponding solution in the Monte Carlo efficiency calculation. The functions $\chi^2(\xi)$ are shown in Fig. 16 for the two solutions. The upper solution gives minima at $\xi = -3.9$ and $\xi = 1.6$ with $\chi^2 = 26$ and 102, respectively. The lower gives solutions with $\xi = -3.8$ and $\xi = 1.3$, with χ^2 of 33 and 112, respectively.

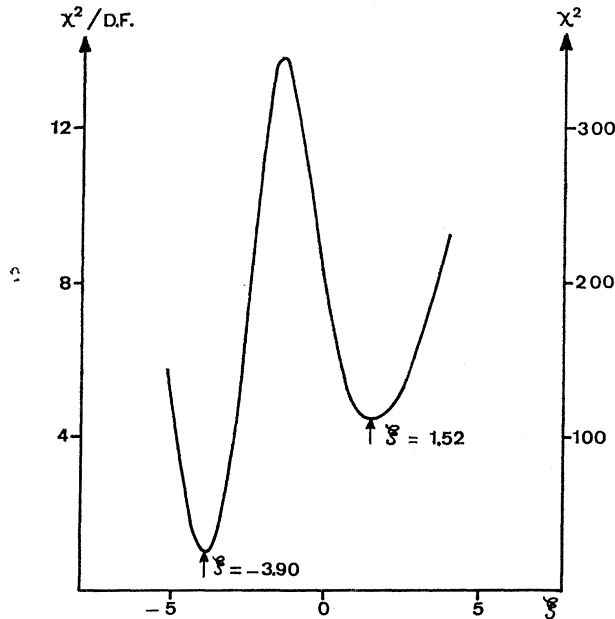


FIG. 13. Plot of χ^2 versus constant ξ obtained from the Dalitz plot for 25 degrees of freedom.

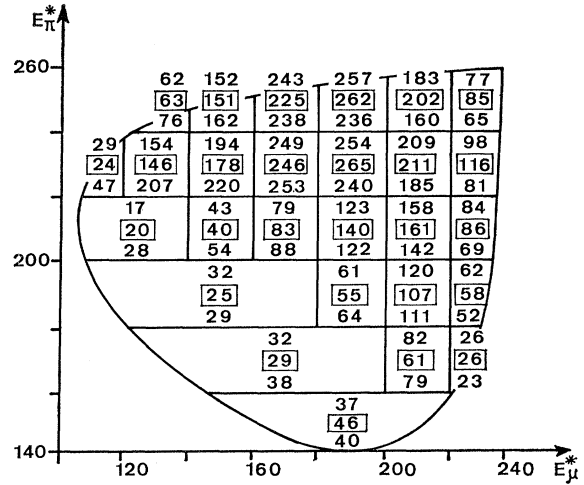


FIG. 14. Expected number of events for each cell of the Dalitz plot for the two solutions. The upper numbers correspond to the solution $\xi = -3.9$ and the lower to $\xi = 1.5$. The experimental numbers are given in the lower boxes. (Energies in MeV.)

We have also examined the sensitivity of the results to a number of other variables. We have found the answers insensitive to variations in the cuts to the data. We have varied the shape of the incident K_L momentum spectrum, with no change in the result. We have found no parameter in the analysis to which the results are sensitive in an important way.

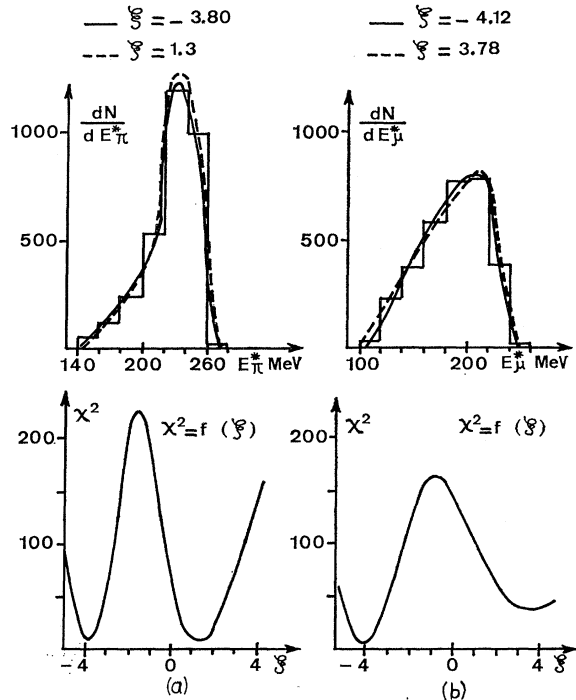


FIG. 15. Separate spectra of pions (a) and muons (b) from the Dalitz plot are given above along with the spectra expected for the two indicated solutions for constant ξ . Below are given the corresponding curves of the function $\chi^2(\xi)$.

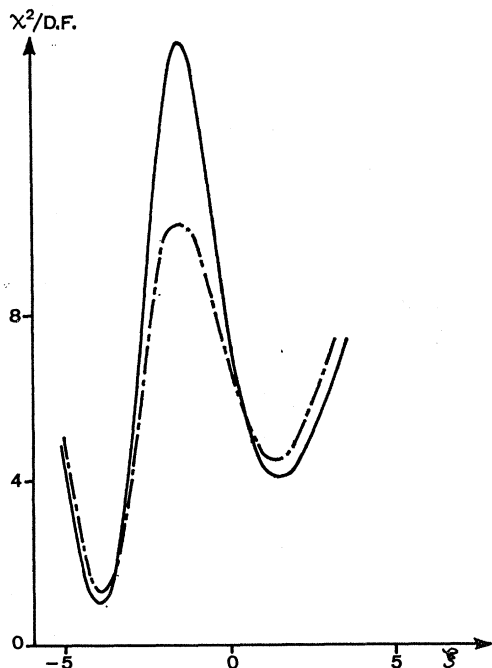


FIG. 16. Plot of the function $\chi^2(\xi)$ for the choice of either the upper or lower solution for the kinematic ambiguity. The upper and lower solutions are given by the solid and dashed lines, respectively.

C. Consideration of q^2 Dependence of ξ

Although the analysis of the Sec. IV B showed that excellent fits could be obtained without invocation of q^2 dependence of the form factors, there are strong reasons for considering such dependences. First, study of $K_L \rightarrow \pi e \nu$ decays indicates a small nonzero value for $\lambda^+ = 0.02 \pm 0.008$. Then it has been suggested by numerous authors^{12,13} that the inclusion of q^2 dependence of form factors could well resolve some of the discrepancies between the various methods of determination of ξ .

The usual formulation of the q^2 dependence of the form factors is made by a linear expansion

$$f_+(q^2) = f_+(0)(1 + \lambda_+ q^2/m_\pi^2)$$

and

$$\xi(q^2) = \frac{f_-(0)(1 + \lambda_- q^2/m_\pi^2)}{f_+(0)(1 + \lambda_+ q^2/m_\pi^2)} \approx \xi(0)[1 + (\lambda_- - \lambda_+)q^2/m_\pi^2].$$

In order to expose a form-factor dependence in the clearest possible way, we have divided the Dalitz plot into three separate energy bands with the ranges

¹² See, e.g., the remarks of N. Cabibbo, in *Proceedings of the Thirteenth International Conference on High-Energy Physics, Berkeley, California, 1966* (University of California Press, Berkeley, 1967), p. 29.

¹³ L. B. Auerbach, A. K. Mann, W. K. McFarlane, and F. J. Sciulli, *Phys. Rev. Letters* **19**, 464 (1967).

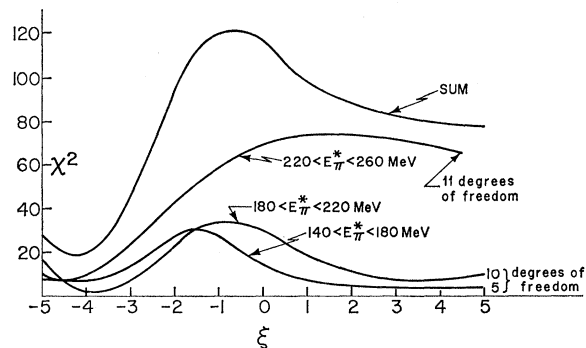


FIG. 17. Plot of the function $\chi^2(\xi)$ for three ranges of E_π^* as indicated. The upper curve is the sum of the three separate curves.

$220 < E_\pi < 260$ MeV, $180 < E_\pi < 220$ MeV, and $140 < E_\pi < 180$ MeV. These ranges correspond to average values of q^2/m_π^2 of 1.4, 3.4, and 5.4, respectively. For each band, we independently evaluate the value of ξ which gives the best fit. We allow the normalization of each band to be independent. Subsequent inspection of the relative normalization constants for each band gives a measure of the dependence of $|f_+(q^2)|^2$ on q^2 , for the case that ξ itself is independent of q^2 .

Figure 17 shows a plot of the functions $\chi^2(\xi)$ for each band in the Dalitz plot. Table I summarizes the results of these curves. The only solution that is consistent with all three bands is the negative solution. Also it should be noted that the relative normalization has a very small variation with each band. The solutions for ξ show no significant variation with the bands so there is no evidence from this experiment for a strong form-factor variation.

In Fig. 18 we have plotted the experimental muon spectra for each range of pion energy. Also we have plotted the expected number of events for $\xi = -3.9$, $\xi = -1$, and $\xi = +1.5$. Each curve is normalized to the number of experimental events in that band. The form of each of these expected spectra is similar and the value of ξ is determined by the detailed difference between the various curves which is of the order of 10–20%. We note that in all the preceding analysis a value $\xi = -1$ (with small q^2 dependence) is least favored. The relative normalization factors for the case $\xi = -1$ are 1.00, 1.30, and 2.20 for mean values of q^2/m_π^2 of 1.4, 3.4, and 5.4, respectively. A value of $\lambda_+ \sim +0.1$ would be required to explain the normalization varia-

TABLE I. Results of analysis of Dalitz plot by bands of E_π^* .

Band	Solution 1 ξ	χ^2_{\min}	Solution 2 ξ	χ^2_{\min}	Degrees of freedom	Relative normal- ization ($\xi = -4.0$)
$220 < E_\pi < 260$	-4.5 ± 0.4	7.2	$> +10$...	11	1.20
$180 < E_\pi < 220$	-3.5 ± 0.4	3.0	$+3.5 \pm 1.0$	7	10	1.15
$140 < E_\pi < 180$	-4.5 ± 0.5	6.5	$+5.0 \pm 2.5$	3.5	5	1.00

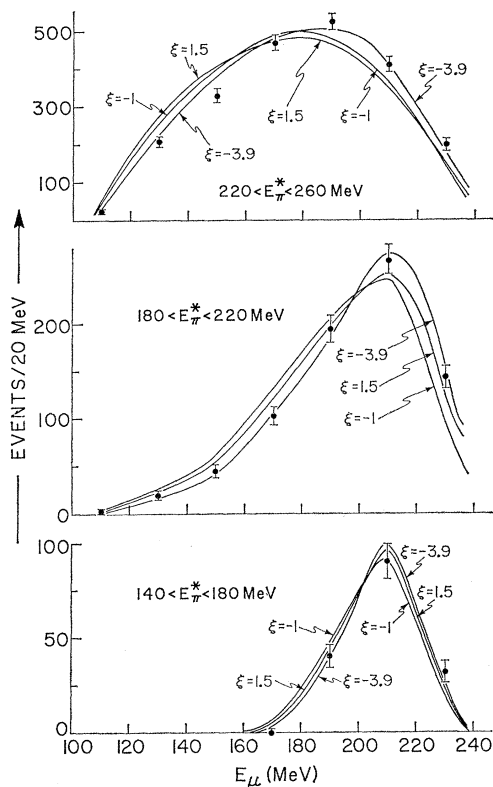


FIG. 18. Plot of the experimental muon spectra for the three bands of pion energy. The solid curves are the expected spectra for the indicated value of ξ . The solid curves are normalized to the experimental curves.

tion. Even with this strong variation one has a $\chi^2=120$ for 26 degrees of freedom.

In Fig. 19 we show the χ^2 as a function of ξ for different bands of pion energy in the case where no q^2 dependence is allowed for either form factor. It is clear that in this case the agreement of the data with $\xi=-1$

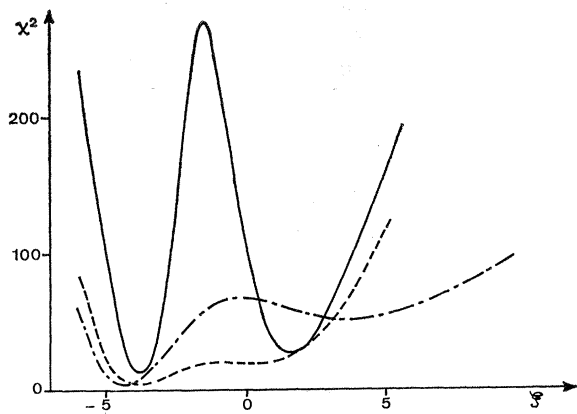


FIG. 19. Variation of χ^2 with respect to ξ for separate bands of pion energy assuming no q^2 dependence for either form factor. The solid, dot-dashed, and dashed curves correspond to the bands $140 < E_{\pi^*} < 220$, $220 < E_{\pi^*} < 240$, and $240 < E_{\pi^*} < 260$, respectively.

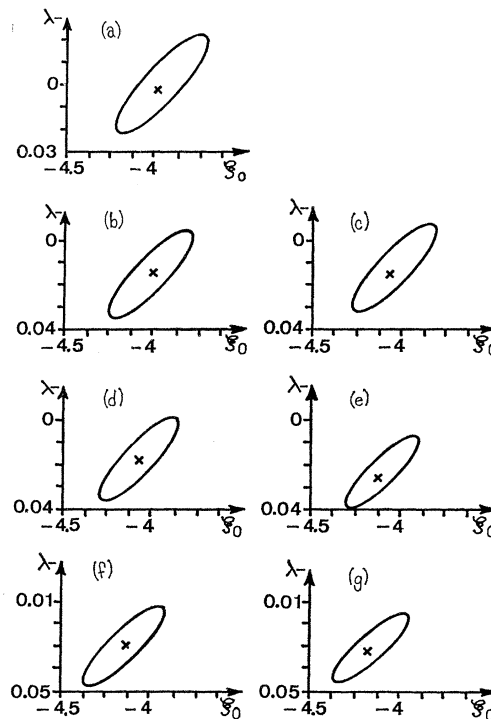


FIG. 20. Curves of $\chi^2_{\min}+1$ as a function of $\xi(0)$ and λ_- with λ_+ as fixed parameter. The position of the χ^2_{\min} is indicated by a cross. The values of χ^2_{\min} are 26.5, 24.3, 22.1, 21.9, 21.8, 22.5, and 24 for $\lambda_+=0.02, 0.01, 0, -0.01, -0.02, -0.03, -0.04$ respectively, for (a)–(g).

is much worse than the case which allows a large form-factor independence.

We have computed χ^2 as a function of $\xi(0)$ and λ_- for fixed λ_+ in order to be more quantitative about the possible form-factor dependence on q^2 . Figure 20 shows the point of best fit and curves of $\chi^2=\chi^2_{\min}+1$ for a series of λ_+ as fixed parameter.¹⁴ An over-all minimum χ^2 occurs for $\lambda_+=-0.015$, $\lambda_-=-0.024$, and $\xi(0)=-4.20$. Here $\chi^2=22$ for 23 degrees of freedom. The errors are highly correlated. For $\lambda_+=+0.02$, any combination of $\xi(0)$ and λ_- such that $\xi(0)+8\lambda_-=-4.0$ will give a reasonable fit for $|\lambda_-|<0.05$. Such a form-factor dependence does not allow a significant change in the value ξ over the physical range of q^2 .

D. Summary

In summary, the data give $\xi(0)=-3.9\pm 0.4$ with no evidence of a strong form-factor dependence. The error is increased to take into account admissible form-factor variations. There is a secondary solution $\xi(0)=1.5$ which is statistically improbable. A value $\xi(0)=-1.0$ is strongly excluded by the data.

¹⁴ Since two parameters are being fitted simultaneously, the contours $\chi^2_{\min}+1$ do not represent 1 standard deviation. The contours $\chi^2_{\min}+2.28$ represent 1 standard deviation.

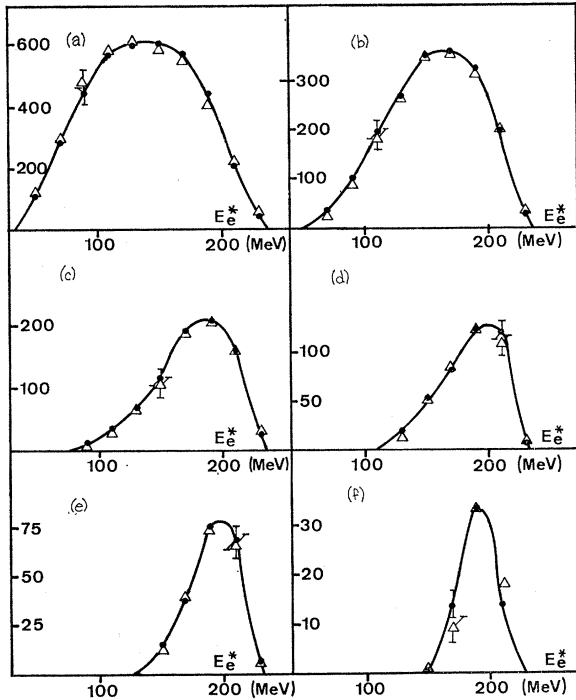


FIG. 21. Electron spectra for K_{e3} events for fixed intervals of E_e^* . The black circles are the experimental points; the triangles are the expected distribution calculated on the basis of a pure vector interaction.

It should be pointed out that our apparatus had a very strong variation of efficiency over the Dalitz plot. Great care was taken in the calculation of this efficiency. The same efficiency calculation was used for the study of $K_L \rightarrow \pi e \nu$ which has already been published.⁸ Figure 21 shows the excellent agreement for the electron spectra in K_{e3} decay for bands of fixed pion energy. The shape of these spectra is entirely determined by the vector interaction which has been confirmed by many experiments. The excellent agreement of these spectra with the prediction serves as a check on our ability to calculate correctly the precise efficiency of our apparatus.

V. MEASUREMENT OF $K_{\mu 3}/K_{e3}$ BRANCHING RATIO

We have also determined $\xi(0)$ by measurement of the branching ratio

$$R = \Gamma(K_L \rightarrow \pi \mu \nu) / \Gamma(K_L \rightarrow \pi e \nu),$$

by means of the relation

$$R = 0.648 + 0.126\xi(0) + 0.019\xi^2(0) + 1.41\lambda_+ + 0.47\lambda_- \xi(0).$$

We have made this measurement in two ways. The first method makes use of a statistical method to separate $K_{\mu 3}$ and K_{e3} . This technique was first used by Adair and Leipuner.¹⁵ For this determination we can

¹⁵ R. Adair and L. Leipuner, Phys. Letters 12, 67 (1964).

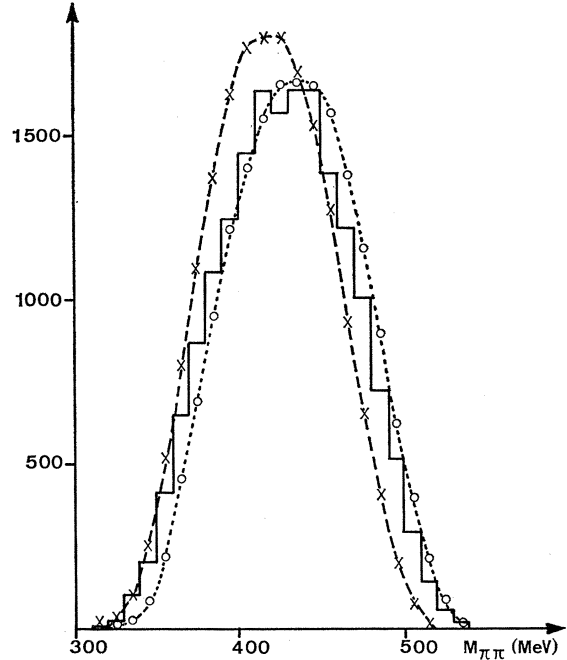


FIG. 22. Histogram of the distribution of $M_{\pi\pi}$ for 17 909 leptonic events. The circles give the distribution expected for K_{e3} and the crosses for $K_{\mu 3}$.

use the complete sample of 17 909 leptonic decays, without regard to information from the range chambers. The contamination of $K_{\mu 3}$ events is negligible because a cut is made so that $P_0'^2 < 0$.

To calculate the fraction n_e of these events that are K_{e3} , we have computed quantities for the events which have different distributions for K_{e3} and $K_{\mu 3}$. These are $M_{\pi\pi}$, the effective mass of the two charged secondaries, assuming that they are π mesons, and $P_0'^2$.

Figures 22 and 23 show the distribution of $M_{\pi\pi}$ and $P_0'^2$, respectively, for the 17 909 events. We have calculated these distributions for K_{e3} and $K_{\mu 3}$ by the Monte Carlo method. We find that the $K_{\mu 3}$ distribution is not sensitive to the assumed value of $\xi(0)$ in the range from +1.5 to -4. The expected distributions for $M_{\pi\pi}$ and $P_0'^2$ for either pure $K_{\mu 3}$ decay or K_{e3} decay are also given in Figs. 22 and 23. These are normalized to the 17 909 events.

We have found the value of n_e which gives the best fit to the observed distributions by a least-squares fit. Table II gives the results. The large χ^2 values are due to bins which are sensitive to a small contamination of $K_{\mu 3}$ events. Elimination of these bins does not change

TABLE II. Statistical separation of K_{e3} and $K_{\mu 3}$.

Distribution	n_e	χ^2	Degrees of freedom
$M_{\pi\pi}$	0.60 ± 0.03	53.5	21
$P_0'^2$	0.62 ± 0.02	51.4	19

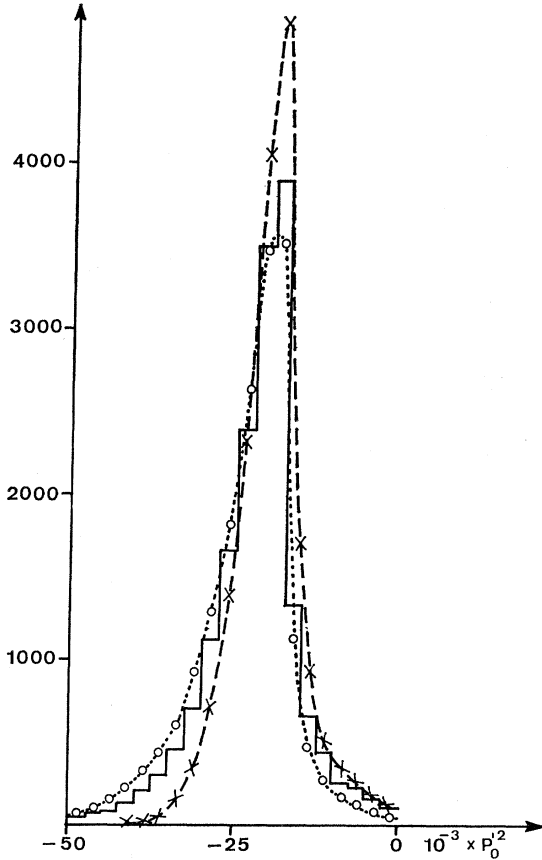


FIG. 23. Histogram of the distribution of $P_0'^2$ for 17 909 leptonic events. The circles give the distribution expected for K_{e3} and the crosses for $K_{\mu 3}$.

n_e . Combining the two results gives $n_e = 0.615 \pm 0.015$ and $R_{\text{expt}} = 0.626 \pm 0.04$.

We have also found R_{expt} more directly by considering the identified events from the subsample of 9382 events for which the range chambers were established to be functioning with high efficiency. Among these events, we identified 5170 K_{e3} and 3548 $K_{\mu 3}$. 664 events could not be identified. By least-squares fit we have found n_e to be 1.00 ± 0.01 , 0.01 ± 0.01 , and 0.55 ± 0.38 , respectively, for the three categories. Combining these fractions gives $R_{\text{expt}} = 0.68 \pm 0.08$, which is consistent with the value established by the completely statistical separation.

In order to relate the experimental ratio to ξ , we have calculated the ratio expected for our apparatus as a function of ξ . The efficiency of the apparatus is itself a function of ξ as well as the real branching ratio. We have chosen to compute directly R_{expt} as a function of $\xi(0)$ and λ_- , where we choose $\lambda_+ = 0.020$.

R_{expt} can be found from

$$R_{\text{expt}} = \frac{\int (Af_+ + Bf_- + Cf_-^2) \epsilon(E_\pi^* E_\mu^*) dE_\pi^* dE_\mu^*}{\int (Af_+^2) \epsilon(E_\pi^*, E_e^*) dE_\pi^* dE_e^*},$$

where the coefficients A, B, C are defined in Sec. I, f_+ and f_- are functions of q^2 as determined by λ_+ and λ_- , and $\epsilon(E_\pi^*, E_\mu^*)$ is the efficiency of the apparatus at the particular point in the Dalitz plot that is determined by the Monte Carlo method. The result of the integration is

$$R_{\text{expt}} = 0.685 + 0.094\xi(0) + 0.014\xi(0)^2 + 0.237\lambda_- \xi(0) + 0.094\lambda_- \xi(0)^2.$$

For a given value of λ_- , $R_{\text{expt}}(\xi_0)$ is a parabola. In Fig. 24, we have plotted this function with λ_- as a parameter. All these curves pass through the same point at $\xi(0) = -2.6$ and, whatever the value of λ_- , we find one value of $\xi(0)$ between -0.5 and -1.0 . The second solution is more strongly dependent on λ_- . To obtain a solution $\xi(0) = -3.9$, we require $\lambda_- \geq 0.14$ which is very large and not compatible with the observed Dalitz-plot distribution.

If we take $\lambda_- = 0$, we find $\xi(0) = -0.50 \pm 0.5$ or $\xi(0) = -6.1 \pm 0.5$. The true value for the observed branching ratio when the experimental efficiency is unfolded is 0.62 ± 0.05 for $\xi(0) = -0.5$ and $\lambda_- = 0$.

VI. CONCLUSIONS

We have measured $\xi(0)$ by two independent methods. By means of the Dalitz-plot distribution we find $\xi(0) = -3.9$. Also we find that the value of the form-factor parameter $|\lambda_-| \leq 0.05$. With the assumption of μ - e universality, the observed branching ratio $\Gamma(K_L \rightarrow \pi\mu\nu)/\Gamma(K_L \rightarrow \pi e\nu)$ determines $\xi(0)$ to be

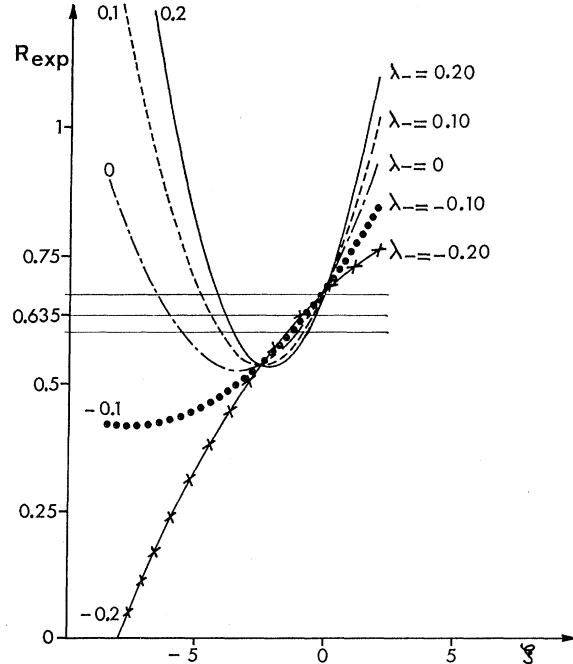


FIG. 24. R_{expt} as a function of $\xi(0)$ and λ_- for $\lambda_+ = 0.023$.

-0.5 ± 0.5 when the form-factor parameter $\lambda_- = 0$. We require λ_- to be ≥ 0.14 to get a solution in agreement with $\xi(0)$. However, this strong form-factor dependence is in contradiction to the dependence allowed by the Dalitz-plot distribution, and contradicts the nature of an expansion in powers of q^2/m_π^2 with small coefficients.

Thus, regardless of any other experimental results, we have an internal contradiction unless we are willing to give up universality. A less drastic conclusion might be related to the manner in which the data have been parametrized. It is conceivable that a more bizarre form-factor variation might account for these results. We cannot completely exclude some experimental difficulty that has gone unnoticed. We are strongly dependent on the detailed accuracy of our efficiency calculation, and it has been impossible to make a direct experimental measurement of this efficiency.

It is often pointed out¹⁶ that the effect of the presence of f_- is to change the Dalitz-plot distribution most strongly in the region of large q^2 . In our apparatus the efficiency falls off rapidly at large q^2 , so that our effective precision for ξ is essentially independent of q^2 . This can be seen from the first column of Table I. Thus, any errors in our efficiency calculation must be so contrived as to give an incorrect value of ξ for all parts of the Dalitz plot.

Inspection of Fig. 18 would indicate that a 3% downward shift of all c.m. energies would lead to better agreement with $\xi = -1$ and, perhaps, better internal consistency with the branching-ratio result. If such an error had been made, one would expect to find the $M_{\pi\pi}$ peak in the regeneration run (Fig. 3) at 485 MeV instead of 500 ± 1.5 MeV.

Table III gives the results of recent determinations of $\xi(0)$ by the various methods. The results for the Dalitz plot are given for $\lambda_+ = \lambda_- = 0$. Inserting the known value of λ_+ for $^*K_{e3}$ under the assumption of universality makes no significant change. The branching-ratio results are obtained with the assumption $\lambda_+ = 0.02$, $\lambda_- = 0$. The polarization results have been obtained for an average over the Dalitz plot such that $\langle q^2/m_\pi^2 \rangle \sim 3$.

The agreement between the various methods of determination of $\xi(0)$ is very poor. This difficulty has been emphasized by a number of authors,^{16,17} and attempts to render the branching-ratio and polarization results compatible have required very large λ_- form factors. At present, the Dalitz-plot data of our experiment and that of Table III, exclude $\xi \approx -1.0$, even though the two experiments are in disagreement.

TABLE III. Recent determinations of $\xi(0)$, assuming $\lambda^+ = 0.02$ and $\lambda^- = 0.00$. Less probable solutions are given in parentheses.

$\xi(0)$	Method	Reference
$+1.2 \pm 0.8$ (-4.0)	Dalitz plot	a
-3.9 ± 0.02 ($+1.5$)	Dalitz plot	present experiment
$-1.81_{-0.26}^{+0.60}$	Polarization	b
-1.2 ± 0.5	Polarization	c
-1.6 ± 0.5	Polarization	d
$+0.3 \pm 0.4$ (-6.80)	Branching ratio	e
$+0.3 \pm 0.3$ (-6.80)	Branching ratio	f
-0.22 ± 0.3 (-6.40)	Branching ratio	g
-0.50 ± 0.5 (-6.10)	Branching ratio	present experiment

^a D. W. Carpenter, A. Abashian, R. J. Abrams, G. P. Fisher, B. M. K. Nefkens, and J. H. Smith, Phys. Rev. **142**, 871 (1966).

^b M. J. Longo, K. K. Young, and J. A. Helland, Phys. Rev. **181**, 1808 (1969).

^c L. B. Auerbach, A. K. Mann, W. K. McFarlane, and F. J. Sciulli, Phys. Rev. Letters **17**, 980 (1969).

^d R. J. Abrams, A. Abashian, R. E. Mischke, B. M. K. Nefkens, J. H. Smith, R. C. Thatcher, L. J. Verhey, and A. Wattenberg, Phys. Rev. **176**, 1603 (1968).

^e I. A. Budagov *et al.*, Nuovo Cimento **57A**, 182 (1968).

^f P. Beilliere *et al.*, Phys. Letters **30B**, 202 (1969).

^g G. R. Evans *et al.*, Phys. Rev. Letters **23**, 696 (1969).

A similar situation has been evident for some time with $K^+ \rightarrow \pi^0 \mu \nu$.¹⁷ The $\Delta I = \frac{1}{2}$ rule requires that the parameter ξ be the same for K^+ and K^0 . The few instances of violation of the $\Delta I = \frac{1}{2}$ rule are small and thus one expects that there will be no significant quantitative difference between K^+ and K^0 . In a recent series of experiments by the X₂ collaboration¹⁸ where K^+ have been stopped in a heavy-liquid bubble chamber, ξ has been measured by all three methods and the results are compatible with $\xi(5.0m_\pi^2) = -0.93 \pm 0.23$, $\Lambda \approx \xi(0)$ ($\lambda_- - \lambda_+$) = $-0.01_{-0.11}^{+0.13}$, and $\lambda^+ = 0.060_{-0.017}^{+0.021}$.

Although the above result indicates that all the difficulties with the $K \rightarrow \pi \mu \nu$ decay will eventually be resolved, data by other experimenters, even for K^+ ,^{1,2} are not in such good agreement. In particular, with the exception of the above-mentioned experiment, discrepancies between the various methods of determination of ξ persist.

Thus it remains to be seen whether there is really anything unusual about $K_{\mu 3}$ decay. The experiment which determines ξ from the Dalitz-plot distribution must be repeated with an improved apparatus which samples the Dalitz plot in a less biased fashion.

ACKNOWLEDGMENTS

We wish to thank our electronics team J. C. Brisson, M. Lemoine, and J. L. Poinignon for their contribution to this experiment and the Saturne operating crew, SEFS, for their splendid cooperation. We also wish to thank Mr. Tsai for his design of the magnets and the group SEFA for their assistance in rapid delivery of the magnets. We also thank the group of "Ariane" for their help in analyzing the pictures.

¹⁸ D. Haidt, J. Stein, S. Natali, G. Piscitelli, F. Romano, J. Lemonne, R. Møllerud, T. I. Pedersen, S. N. Tovey, V. Brisson, L. Kluber, P. Petiau, C. D. Esveld, R. T. Van deWalle, B. Aubert, L. M. Chounet, Dong Le, J. P. Lowys, E. Calimani, S. Ciampolillo, F. Mattioli, F. Sconza, D. Gamba, and A. Marzari-Chiesa, Phys. Letters **29B**, 696 (1969).

¹⁶ See, for example, C. Rubbia, in Proceedings of the Topical Conference on Weak Interactions, CERN, 1969, p. 227 (unpublished) (CERN Report No. 69-7, available from CERN, Scientific Information Service, Geneva).

¹⁷ W. J. Willis, in *Proceedings of the International Conference on Elementary Particles, Heidelberg, 1967* (North-Holland, Amsterdam, 1968), p. 273.

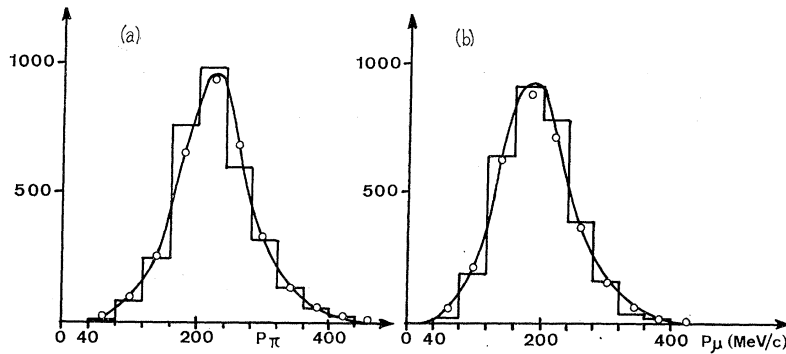


FIG. 25. Comparison of Monte-Carlo-generated and observed laboratory momentum spectra for pions (a) and muons (b). The histograms are the experimental distribution and the circles are the calculated distributions.

APPENDIX: MONTE CARLO PROGRAM

The efficiency of the apparatus was calculated by the Monte Carlo method. $K_{\mu 3}$ events were selected uniformly in the Dalitz plot and all the experimental conditions were reproduced. The K_L spectrum was first chosen, based on the calculations of Block¹⁹ and the measurements of Piroué and Smith,²⁰ on the production of K^+ at 90° at the Princeton-Pennsylvania Accelerator. Included in the calculation were the geometry of the apparatus and the magnetic field, including the effect of the fringe fields and vertical focusing. Decays in flight were included. Errors due to multiple scattering and measurement were included and their magnitude was verified by the run with a copper regenerator. The effects of the trigger logic were included.

Once the simulated events were established in the laboratory, the same programs used in the analysis of the true events were used to reconstruct the simulated events. Identical cuts were applied to the true and Monte-Carlo-generated events. In general one finds that if an event was originally chosen by the Monte Carlo method (or actually produced in the experiment) with energies $E_\pi^*(1)$ and $E_\mu^*(1)$, they will be found at different energies $E_\pi^*(2)$ and $E_\mu^*(2)$. A large sample of such Monte Carlo events was generated to be used to compute any desired distribution as a function of ξ .

To illustrate the technique, consider the case for which ξ is independent of q^2 . Then the events are dis-

tributed according to

$$N(E_\pi^*, E_\mu^*) = A + B\xi + C\xi^2,$$

where A , B , and C are the functions of E_π^* and E_μ^* given in Sec. I. We consider the first term. N^A events are chosen over the Dalitz plot with a weight $A(E_\pi^*, E_\mu^*)dE_\pi dE_\mu$. Among these selected events, M_j^A are found on reconstruction in a particular cell j of the Dalitz plot. The cell j is usually a 20×20 -MeV area specified by central energies $E_\pi^*(j)$ and $E_\mu^*(j)$. We define A_j to be the ratio $M_j^A/N^A = A_j$. Coefficients B_j and C_j are defined in a similar way. Then the number of events observed in a cell j for given value of ξ is given by

$$N_j = K(A_j + B_j\xi + C_j\xi^2),$$

where K is a normalizing factor such that $\sum N_j$ equals the total number of events in the sample. The procedure that was followed when form factors were inserted was similar.

There were a number of ways by which the accuracy of the efficiency calculation was checked. The agreement of the electron spectra in K_{e3} has already been shown in Fig. 21 and represents the most exacting test of the calculation. The agreement with the P_0^2 distribution and P_T distribution for identified $K_{\mu 3}$ events shown in Fig. 8 is another confirmation of the calculation. Finally, the prediction of the laboratory spectra for the pions and muons is least sensitive to the details of the decay interaction while still sensitive to parameters in the Monte Carlo calculation. These comparisons between experiment and the Monte Carlo method are shown in Fig. 25.

¹⁹ M. M. Block, E. M. Harth, and R. M. Sternheimer, Phys. Rev. 100, 324 (1955).

²⁰ P. A. Piroué and A. J. S. Smith, Phys. Rev. 148, 1315 (1966).